ELSEVIER

Journal of Neuroscience Methods 102 (2000) 177–186

JOURNAL OF NEUROSCIENCE METHODS

www.elsevier.com/locate/jneumeth

A robotic manipulator for the characterization of two-dimensional dynamic stiffness using stochastic displacement perturbations

Ana Maria Acosta, Robert F. Kirsch *, Eric J. Perreault

Department of Biomedical Engineering, Case Western Reserve University, and Cleveland VA FES Center, 407 Wickenden Building, Cleveland, OH 44106, USA

Received 17 March 2000; received in revised form 24 July 2000; accepted 25 July 2000

Abstract

Experimental techniques for estimating the two-dimensional dynamic stiffness of the human arm over a wide range of conditions have been developed. A robotic manipulator has been developed to create loads against which subjects perform various tasks and also to impose perturbations onto the endpoint of the arm to allow estimation of its mechanical properties. The manipulator can produce static endpoint forces exceeding 220 N in any direction in its plane of motion, and this plane can be vertically translated and tilted over wide ranges to study arm dynamic stiffness in many functionally relevant planes. It can impose stochastic position and force perturbations whose bandwidth exceeds that of the arm. These random perturbations avoid undesirable volitional reactions and allow the efficient estimation of stiffness dynamics using experimental trials of short duration. The ability of this manipulator to characterize inertial-viscoelastic systems was tested using several two-dimensional physical systems whose properties were independently characterized. The endpoint dynamic stiffness properties of a human arm were estimated as an example of the use of the manipulator in studying upper limb mechanical properties. The system properties characterized by these methods will be useful in probing normal neural arm control strategies and in developing rehabilitation interventions to improve arm movements in disabled individuals. © 2000 Published by Elsevier Science B.V.

Keywords: Human arm; Motor control; Endpoint stiffness; Robot manipulator; Viscoelasticity; Multi-joint; Neuromuscular; Stochastic perturbations

1. Introduction

Human movements are produced by muscle contractions that generate enough force to move the limbs against external loads. Muscles also generate stiffness, a stabilizing influence that provides resistance to external disturbances and thus helps maintain the limb in the intended locations or on the desired movement trajectory. Stiffness is typically defined statically as the relationship between an imposed displacement and the evoked force, similar to a spring. Several muscle mechanisms contribute to static stiffness, including length–tension properties (Matthews, 1959; Gordon et al., 1966; Rack and Westbury, 1969; Crago et al., 1976), crossbridge elasticity (Ford et al., 1981; Kojima et al., 1994; Huxley, 1995) and the tonic stretch reflex (Nichols and Houk, 1973, 1976; Houk, 1979; Hoffer and Andreassen, 1981). However, the resistance generated by the limb in response to external perturbations also has important dynamic components (Hogan, 1985; Kearny and Hunter, 1990), including the inertia of the limb and the viscous properties of muscles.

The dynamic stiffness properties of a limb as a whole are more complex than those of individual muscles or joints for several reasons. In both the human upper and lower extremities, several muscles cross more than one joint, inherently coupling the actions of the various joints. Even in the absence of multi-joint muscles, the geometric properties of the limb require coordination between the different joints in order to achieve a desired endpoint location. Dynamically, significant mass-related interaction moments (inertial, centripetal and coriolis) between different limb segments occur during many movements (Hollerbach and Flash, 1982; Lac-

* Corresponding author. Tel.: +1-216-3683158; fax: +1-216-3684969.

E-mail address: rfk3@po.cwru.edu (R.F. Kirsch).

0165-0270/00/$ - see front matter © 2000 Published by Elsevier Science B.V.
PII: S0165-0270(00)00307-1

quaniti and Soechting, 1986a). Reflex responses of both mono- and bi-articular muscles appear to depend on the motion of the entire limb and not only on the changes in length and tension of a particular muscle (Lacquaniti and Soechting, 1986b; Soechting and Lacquaniti, 1988). Because of these properties, an applied endpoint displacement will usually result in a force response that is not directly opposed to the applied displacement, but rather will have components in other directions as well. The directional properties of endpoint elasticity, viscosity, and inertia are best described using matrix notation rather than scalars (Hogan, 1985; Mussa-Ivaldi et al., 1985).

Considering these properties, any apparatus used to examine multi-joint dynamic stiffness properties must be capable of imposing perturbations with an adequate bandwidth in more than one spatial direction and must also be capable of measuring the resulting multi-dimensional responses. Beginning with the pioneering work of Mussa-Ivaldi et al. (1985), multi-joint posture and movement control has been the focus of an increasing number of research studies in recent years. Two degree-of-freedom robotic manipulators have been used in such studies to impose perturbations onto the endpoint of the arm in order to characterize its planar (i.e. two-dimensional) stiffness properties during posture (Mussa-Ivaldi et al., 1985; Shadmehr et al., 1993; Tsuji et al., 1995; Gomi and Osu, 1998; Osu and Gomi, 1999) and movement (Gomi and Kawato, 1996, 1997). Mussa-Ivaldi et al. (1985) characterized the static stiffness generated in response to step displacements imposed in several different directions. Although this study established the concept and basic experimental approach to estimating planar stiffness, the one trial per perturbation direction approach is tedious and relies on trial-to-trial repeatability. Furthermore, the manipulator used was not powerful enough to impose significant loads as well as perturbations. Tsuji et al. (1995) used a direct drive two-joint planar manipulator to characterize the dynamic stiffness of the arm by imposing small position perturbations onto the endpoint of the limb, while the subject maintained a given posture. Gomi and Kawato (1996, 1997) developed a parallel link drive, air-magnet floating planar manipulator to characterize the stiffness of the human arm during multi-joint point-to-point movements by applying short position perturbations during the movement. In the same laboratory, Osu and Gomi (1999) investigated changes in the viscoelastic properties of the human arm on the horizontal plane during cocontraction and force regulation tasks. Shadmehr et al. (1993) used a planar manipulator to produce a viscous force field to study motor learning during arm reaching movements. Milner and Cloutier (1993) studied wrist movement stability by applying loads with negative viscosity that reduced the damping of the wrist. These studies have used unnatural loads to examine the ability of the nervous system to adapt when the dynamics of the arm are changed. Other studies (McIntyre et al., 1996) have imposed constant force loads using weights to simulate common natural conditions, for example the effects of gravity on masses held in the hand. Xu et al. (1991) designed an airjet perturbation device to determine the mechanical properties of the human arm during unconstrained posture and movement, by imposing stochastic perturbations onto the wrist. This group reported results on the mechanical properties of the human elbow joint during posture (Xu et al., 1991; Xu and Hollerbach, 1998), and slow (Xu and Hollerbach, 1999) and cyclic movements (Bennett et al., 1992), characterized using the airjet device. Although this device can potentially impose perturbations in three orthogonal directions, only one-dimensional studies have been reported. Also, the maximum forces that can be imposed with this device are very low (4 N), limiting the ability to explore the effect of loads on the mechanical properties of the human arm.

These studies have examined a relatively small range of conditions because of the restricted capabilities of the manipulators used. Typically, only small loads have been imposed due to limitations in manipulator strength. Transient perturbations such as steps have been used almost exclusively, requiring one trial per direction of interest, which becomes very tedious if adequate positional resolution is to be obtained for several experimental conditions. This approach also assumes that the subjects perform identically over the course of many trials.

This report describes a manipulator that can produce significant force in any direction throughout its planar workspace and has a position bandwidth sufficient to fully describe the dynamic properties of the human arm. Its plane of movement can be translated up and down, as well as inclined over a wide range to allow the study of arm dynamics in planes other than shoulder-level horizontal. The ability of this manipulator, when used in conjunction with a multi-input, multi-output system identification procedure (Perreault et al., 1999), to accurately characterize the mechanical properties of several known physical systems is demonstrated. In addition, an example of human arm dynamic endpoint stiffness is included.

Portions of this work have appeared previously in abstract form (Acosta and Kirsch, 1996a,b).

2. Manipulator design and instrumentation

2.1. Manipulator design

The manipulator illustrated in Fig. 1 is a two degree-of-freedom planar robotic arm designed by the authors

in conjunction with the manufacturer (Mahar-Spar Inc., Cleveland, OH). The robotic arm consists of two links, two motors, and the cable transmission connecting the links and motors. The links are very rigid yet lightweight because of the fiberglass composite material used in their construction. The two motors are standard 7″ dc servo motors (Gettys, Inc. M238), each capable of exerting a maximum continuous torque of 30 N·m when powered by their motor controllers (Gettys, Inc. A243/CLX-30 A). These amplifiers utilize internal current feedback to improve the accuracy of the torque output from the motors.

Each motor drives a separate joint via nylon-coated 3.175 mm diameter steel cable transmissions, allowing independent control of each joint. One of the motors drives the inner joint of the manipulator through a pair of cables attached in a push-pull manner to a 7.62 cm pulley mounted to the motor shaft and a 15.24 cm pulley attached to the inner arm segment and aligned with its center of rotation. The transmission ratio for the inner joint is thus 2:1, doubling the torque to compensate for the longer moment arm through which it must act. The second motor drives the outer joint of the manipulator through a two-stage transmission. A 7.62 cm pulley concentric (but rotationally independent) with the inner joint is connected to the motor through a pair of cables as was the case for the inner joint. A shaft connects this pulley with an identical pulley vertically centered within the inner arm segment. This pulley is connected by a pair of cables to an identical pulley that is attached to the outer arm segment and aligned with its center of rotation. The first-stage cables from the motors are pre-tensioned using turnbuckles connected in series. The second-stage cables for the outer joint transmission are pre-tensioned using a pair of idler pulleys mounted on a slider mechanism. Cable tension is adjusted to eliminate backlash while minimizing bearing friction.

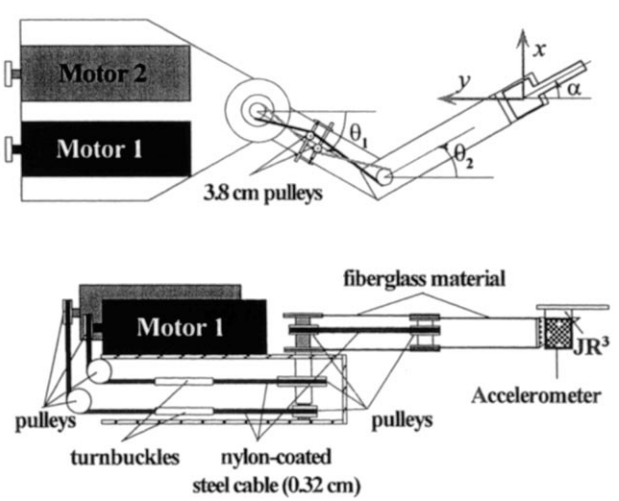

Fig. 1. Two-degree of freedom manipulator for measuring the mechanical properties of the human arm. The links are driven by two dc motors with a cable transmission connecting the motors to the joints.

The arm and the motors are mounted on a steel platform that is supported between two large steel columns. The inclination of the platform can be adjusted over a range of -90 to 80° relative to horizontal using a rotary table attached to the platform. The weight of the platform, motors, and rotary table (~ 340 kg) is balanced by a counterweight of approximately the same mass housed in one of the columns and attached to the platform via a steel chain transmission. The counterweight allows the manipulator arm to be raised and lowered with minimum effort over a vertical range of 80 cm. Once the platform is adjusted to the desired height, it is friction-clamped to each of the vertical columns to rigidly hold it in place.

2.2. Instrumentation

The manipulator is instrumented with rotary encoders mounted at each joint, and a six-axis force-moment transducer and a three-axis accelerometer mounted at the endpoint. Manipulator joint angle signals (used for manipulator control and data recording during experiments) are measured using rotary encoders (Dynamics Research Corporation, Model 153, 5000 counts per revolution) mounted at each joint. Endpoint forces exerted by the manipulator on an external object (typically a human arm) are measured using a six-axis force transducer (JR^3, Inc., Model 30E15A-U560A) mounted at the endpoint of the manipulator (maximum range ± 334 N in the plane of the manipulator, ± 668 N in the orthogonal direction). The force transducer is mounted on a bearing that allows free rotation about the axis orthogonal to the plane of motion to prevent unwanted twisting of the subject's arm due to the linear movement of the manipulator. The angle of this rotation (designated as α) is measured with a potentiometer referenced to the outer link (see Fig. 1) and used to transform the measured forces from the rotating coordinate frame of the transducer into the fixed coordinate frame of the manipulator. Finally, a three-axis linear accelerometer (Analog Devices, Model ADXL05) with a range of ± 5 g on each axis is mounted at the endpoint directly beneath the force transducer to measure endpoint accelerations.

2.3. Safety

Several redundant safety systems have been implemented. A 2.54 cm ball caster is attached to the base of the endpoint of the manipulator and rolls smoothly along the bottom of a square box that acts as a hard stop and also prevents any vibration in the direction orthogonal to the plane of motion. The endpoint of the manipulator is constrained to move within the area

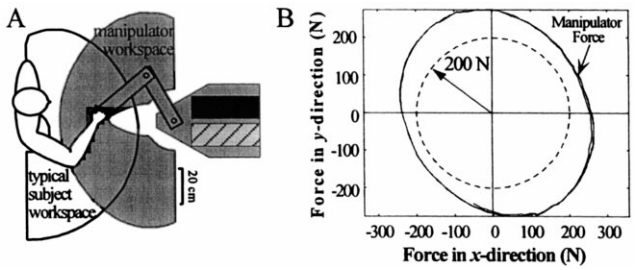

Fig. 2. Manipulator capabilities. (A) Workspace of the manipulator compared to the functional workspace of an average able-bodied male. (B) Endpoint force produced by the manipulator (solid trace) which exceeded 220 N in every direction.

defined by a set of four adjustable bars within the box. In addition to this physical stop, the subject or the experimenter holds a 'momentary' switch that must be actively and continuously depressed during an experiment to complete the enable circuit of the motor amplifiers. Software safety algorithms have also been implemented, disabling the motor amplifiers if the endpoint of the manipulator moves outside a circle with a 6-cm radius centered at the desired endpoint position. Finally, human subjects are positioned so that the manipulator cannot reach their bodies even if an unprecedented failure of all of the other safety features occurs.

2.4. Control

A closed-loop endpoint position and velocity (PD) controller for the manipulator has been implemented using a floating-point digital signal processing (DSP) board (Spectrum Inc. model PC/C31 real-time application board, 40 MHz) within an IBM-compatible computer. The DSP board samples the control signals (desired joint angles) with 12-bit resolution at 3 kHz, and computes and outputs the motor voltage commands required to produce the desired position at the same rate. The controller gains (proportional and derivative) were set to obtain maximum stiffness without instability. This stiffness is directional because of the geometry of the manipulator, but its range (8000–66 000 N/m) is considerably higher than the expected stiffness of the human arm.

3. Manipulator capabilities

3.1. Workspace

The range of motion of the manipulator is planar (i.e. two-dimensional) and is roughly semi-annular in shape, with an outer radius of 70 cm and a 10 cm inner radius as shown by the shaded region in Fig. 2A. When compared to the workspace of an able bodied person in a horizontal plane at shoulder level (unshaded region in Fig. 2A), it is evident that the manipulator covers a significant fraction of this functional workspace. By appropriate positioning of the subject relative to the manipulator, all reachable human arm postures in this plane and most planar arm movements, can be examined using the manipulator. As noted above, the plane of motion of the manipulator can be raised and lowered over an 80-cm range, as well as inclined over a range of $\sim 170°$ centered at horizontal.

3.2. Force range

Based on the maximum torque ratings of the motors, the manipulator is theoretically capable of producing forces with magnitudes of more than 350 N in any direction for a typical geometrical configuration of the robotic arm ($\theta_1 = -45°$, $\theta_2 = 45°$). Such force magnitudes are in excess of the range of our current force transducer and also beyond the range of any anticipated experimental paradigm. Fig. 2B, therefore, illustrates a slowly varying, submaximal (for the manipulator but within the range of the force transducer) force generated by the manipulator with its endpoint fixed to a rigid stop. The dotted circle in Fig. 2B indicates a 200 N force in each direction in the plane, while the more ovoid (unfilled) curve are the forces generated by sinusoidal (0.1 Hz) voltage commands applied to each of the two motors (90° out of phase). The force measured at the endpoint of the manipulator was greater than 220 N in all directions and approached 300 N in some directions. These force levels are sufficient to simulate most activities of daily living, considering that average males can exert maximum forces of 670 N directed towards the torso in a horizontal plane (Chaffin and Andersson, 1991).

4. Characterization of physical systems

The primary intended use of the manipulator described in this paper is to identify the unknown stiffness dynamics of the human arm under a number of different conditions. In this study, the experimental and analytical methods we will use in future studies are shown to be capable of accurately characterizing several known physical systems and of obtaining estimates of human arm endpoint dynamic stiffness.

4.1. General methods

Three mechanical systems, as well as the human arm, were characterized using perturbations imposed by the manipulator: a two-dimensional spring-mass system, a two-dimensional spring-mass system with a viscosity in one direction, and a single dimensional mass system.

For each of these systems, the manipulator was used to impose independent, bandlimited stochastic displacements in each of its two directions. The amplitude of the perturbations (4 cm peak-to-peak) were chosen to limit the endpoint displacements to an area that has been shown to be appropriate for studies of the human arm (Lacquaniti and Soechting, 1986b). The displacement perturbation was pre-filtered so that the resulting force spectrum was flat over a bandwidth of 20 Hz. This bandwidth is within the physiological range for arm disturbances (Kirsch and Rymer, 1992; Kirsch et al., 1994) but still exceeds the natural frequency of the human arm (~ 2–3 Hz) to allow full characterization of its dynamic properties. The imposed endpoint displacements and the evoked forces were sampled at 500 Hz using a National Instruments AT-MIO-64E-3 analog to digital conversion board housed within an IBM-compatible computer. Two-dimensional dynamic stiffness estimates were obtained using the frequency domain multi-input multi-output identification method described by Perreault et al. (1999). The inputs to this identification procedure were the displacement signals in each of the two orthogonal directions within the plane of movement, and the outputs were the forces measured in the same directions. The identification method produces a set of four input-output frequency responses, one for each combination of the two inputs and the two outputs. Thus, transfer functions relating x displacement to x force, x displacement to y force, y displacement to x force, and y displacement to y force were estimated. In addition, partial coherence functions were generated for each of the four frequency responses, and multiple coherence functions were generated for each of the two output forces. The partial coherence functions indicate how well a given output is linearly predicted by a given input after the effects of all the other inputs are removed from both the input and the output. The multiple coherence functions indicate how well a particular output is predicted by all the inputs. A coherence value of 1.0 indicates a perfect linear relationship, while values lower than 1.0 can indicate non-linearity, noise, estimation bias, or the effects of additional unmeasured inputs.

Second order (mass–spring–dashpot) models were fit to the diagonal elements of the endpoint dynamic stiffness of the elastic and inertial systems using a Nelder–Mead simplex (direct search) method (Lagarias et al., 1998) to minimize the square error between the magnitude of the identified frequency response and the second order model. The air dashpot used in the elastic system with damping was modeled as a Maxwell solid (dashpot in series with a spring) resulting in a third order model that was fit to the identified transfer functions. The model parameters were then compared with the 'actual' values of the parameters (two-dimensional stiffness of the springs, viscosity of the dashpot, and weight of the mass) to determine the accuracy of the experimental and analytical approaches. Second order models were also fit to the elements of the human arm endpoint dynamic stiffness and the estimated parameters were compared to those reported in previous studies under similar conditions.

4.2. Elastic system

Fig. 3A illustrates a two-dimensional elastic stiffness field generated by a set of four linear mechanical springs with known spring constants attached to the endpoint of the manipulator. The magnitude of this stiffness field was comparable to the endpoint stiffness of the human arm as measured in previous studies (Mussa-Ivaldi et al., 1985; Tsuji et al., 1995). Fig. 3B shows the position perturbations imposed upon these springs, as well as the resulting forces. Fig. 3C shows the transfer functions estimated for each of the four stiffness components (thin solid lines), and the second order fits to these transfer functions (heavy dashed lines). Also shown are the partial and multiple coherence functions, as well as the 'actual' (K_{expected}) and estimated (K_{fit}) elastic stiffness values. Although intended to be a purely diagonal system (i.e. pure x forces produced pure x displacements and pure y forces produced pure y displacements), slight differences in the spring constants of the four springs, as well as their physical arrangement, led to modest and slightly asymmetrical off-diagonal terms. These were much smaller in magnitude than the diagonal terms, and the coherence of the identified off-diagonal transfer functions were significantly lower, as expected. Therefore, no fitted responses are illustrated for the off-diagonal responses. The partial coherence functions for the diagonal components were very close to 1.0 over most of the system bandwidth. The gain and phase of these diagonal terms were not constant across frequency as expected for a purely elastic system because of the mass of the springs, creating a highly resonant mass-spring system that resulted in low coherence around the resonant frequency (~ 4 Hz). However, the estimated elastic stiffnesses of the diagonal elements ($K_{xx} = 384.7$ N/m and $K_{yy} = 356.7$ N/m) were within 9% or less of the expected values ($K_{xx} = 354.3$ N/m and $K_{yy} = 382.0$ N/m).

4.3. Elastic system with damping

A precision air dashpot (Airpot Corporation, Model S444A315X) was added in parallel to the x axis of the elastic system described in the previous section to determine the accuracy with which viscous properties could be estimated. Perturbations and analysis methods identical to those used with the elastic system were again employed here. The diagonal dynamic stiffness fre-

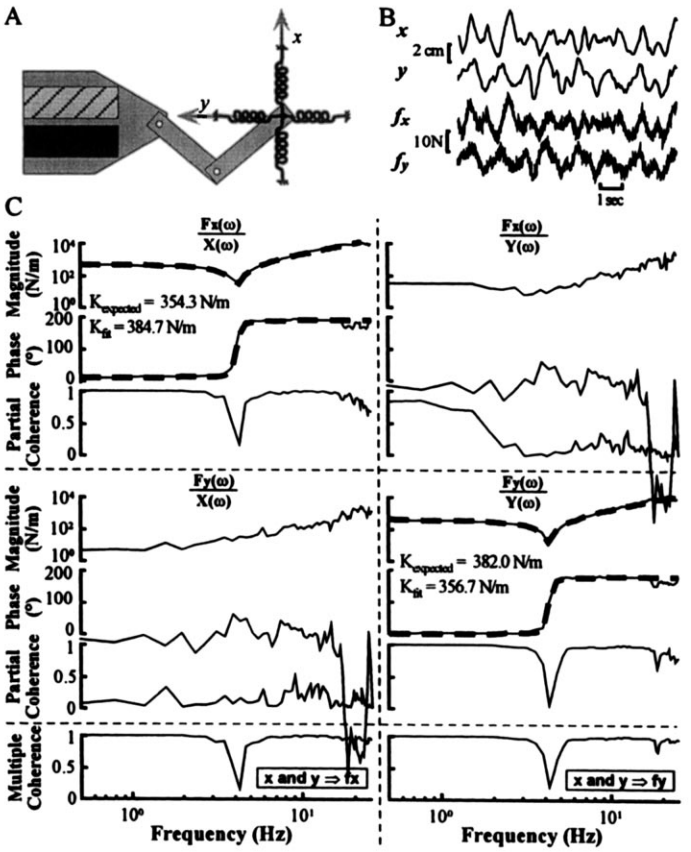

Fig. 3. Identification of an elastic system. (A) Schematic of the manipulator and the experimental setup. (B) Endpoint displacement perturbation and resulting force in each of the two orthogonal directions. (C) Elements of the elastic field represented by their frequency responses (magnitude and phase) with the corresponding partial coherence and multiple coherence functions. The second order fits for the diagonal elements are illustrated by the dashed traces.

quency responses and corresponding partial coherences obtained from this system are shown in Fig. 4. The *yy* dynamic stiffness component exhibited the same undamped responses seen for the elastic system of Fig. 3, but the *xx* dynamic stiffness was, as expected, highly damped. The off-diagonal terms were again much smaller in magnitude and estimated with much lower coherence than the diagonal terms, and the estimated diagonal elastic parameters were again within 9% of their actual values. The estimated *yy* viscosity ($B_{yy} = 3.3$ N·s/m) was very near the expected value of zero, while the *xx* viscosity estimate ($B_{xx} = 86.2$ N·s/m) was within 7% of its expected value of 80 N·s/m. Thus, viscous properties can be accurately estimated and viscous properties in one direction do not distort elastic stiffness estimates in the orthogonal direction.

4.4. Inertial system

In this experiment, different masses ranging from 0.3 to 2.54 kg were attached to the force transducer at the endpoint of the manipulator, and similar methods were again used to obtain stochastic endpoint displacement and force data for the identification algorithm. The diagonal components of the endpoint 'stiffness' for a 2.54-kg system are illustrated in Fig. 5; note that this system is again theoretically diagonal in nature. Across the range of high coherence (approximately equal to 1.0

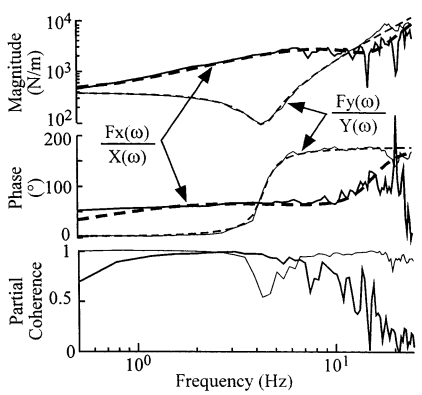

Fig. 4. Identification of a damped elastic system. Diagonal elements of the viscoelastic field represented by the magnitude and phase of the frequency responses with the corresponding partial coherence functions. The dashpot was aligned with the *x*-axis of the system. The transfer functions obtained from the estimated parameters are illustrated by the dashed traces.

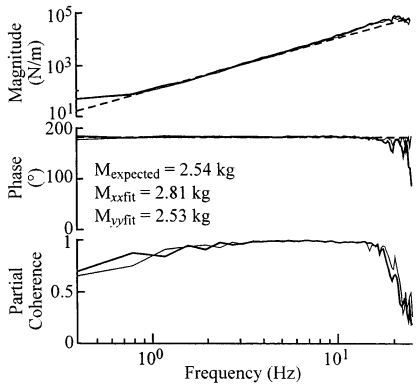

Fig. 5. Identification of a mass. Diagonal elements of the inertial matrix represented by the frequency responses and the partial coherences resulting from the identification procedure. The dashed traces correspond to the frequency response of the actual mass of the object.

over a bandwidth of 1–20 Hz), the frequency responses show the expected 180° phase advance and the monotonic increase in magnitude with frequency. Fitting a mass to these responses resulted in inertial estimates of $M_{xx} = 2.81$ and $M_{yy} = 2.53$, within 11 and 0.3% of the actual mass, respectively. Overall, the errors in the estimates of different masses varied from 0.2 to 11% as can be seen in Fig. 6.

4.5. Human arm

The endpoint dynamic stiffness properties of the arm measured here are only an example of the wide range of conditions that can be tested with the manipulator. The subject was seated facing the manipulator with the right arm in the horizontal workspace at shoulder height. The location of the hand was ~ 0.3 m in front of the shoulder (shoulder angle = 23° from the coronal plane and elbow angle = 125° from full extension). Shoulder straps were used to minimize movement of the trunk, and a fiberglass cast was used to immobilize the wrist and to provide an interface between the subject's hand and the endpoint of the manipulator. During the measurements, the subject was instructed to exert a constant force (24 N) against the manipulator in the x direction (see Fig. 3A). Visual feedback of the endpoint force and the force target were provided to assist the subject in the task. Stochastic perturbations were then applied to the hand, while the subject maintained the constant force for a total of 35 s.

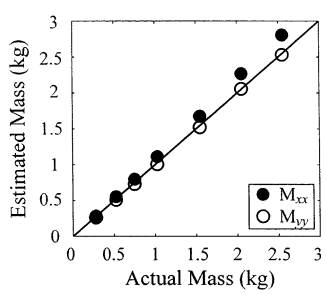

Fig. 6. Inertial estimates of seven different objects obtained from least squares fits to the diagonal elements of the identified frequency responses (closed and open circles). The estimate errors ranged from 0.3 to 11% for the heaviest object (xx element).

Fig. 7 shows the estimated dynamic endpoint stiffness transfer functions. The overall characterization of arm endpoint dynamic stiffness was very good, as reflected by the high multiple coherence values between 1 and 30 Hz. The individual elements were also accurately identified, as evidenced by the high (greater than 0.9) partial coherence functions of all four elements for most of the frequency range of interest. The decline in the partial coherence functions above 10 Hz is due to a deliberate decrease in displacement power at higher frequencies. The diagonal terms exhibited somewhat higher partial coherence functions due to the larger diagonal stiffness magnitudes and accompanying higher signal-to-noise ratio of the measured forces.

The frequency responses (solid traces in Fig. 7), show the decrease in magnitude and the 180° phase shift near 2 Hz suggestive of resonant second order systems. Fits of a second order model to the frequency responses are shown by the dashed traces in Fig. 7. The four sets of parameters from the second order models of the four frequency responses are indicated in each of the panels of Fig. 7 and represent the elastic, viscous and inertial components of the endpoint dynamic stiffness of the arm in two dimensions. The elastic, viscous, and inertial parameters identified for the condition tested are comparable to those identified by others under similar posture conditions although this loading condition has not been reported in previous studies (Mussa-Ivaldi et al., 1985; Tsuji et al., 1995). In summary, the high coherence values and the goodness of fit of the second order models, indicate that the proposed method does an excellent job in characterizing endpoint dynamic stiffness properties.

5. Discussion

We have developed a new approach for studying the stiffness properties and neural control of the human upper limb during posture and movement. The two-degree of freedom manipulator described in this paper can generate position perturbations with a bandwidth exceeding the natural frequency of the human arm, allowing accurate characterization of its dynamic properties (inertia and viscosity) in addition to the static properties (stiffness) as in previous studies. The manipulator is also capable of producing substantially greater endpoint forces than those used in previous studies, allowing characterization of human arm endpoint stiffness during a much wider range of levels of muscle contrac-

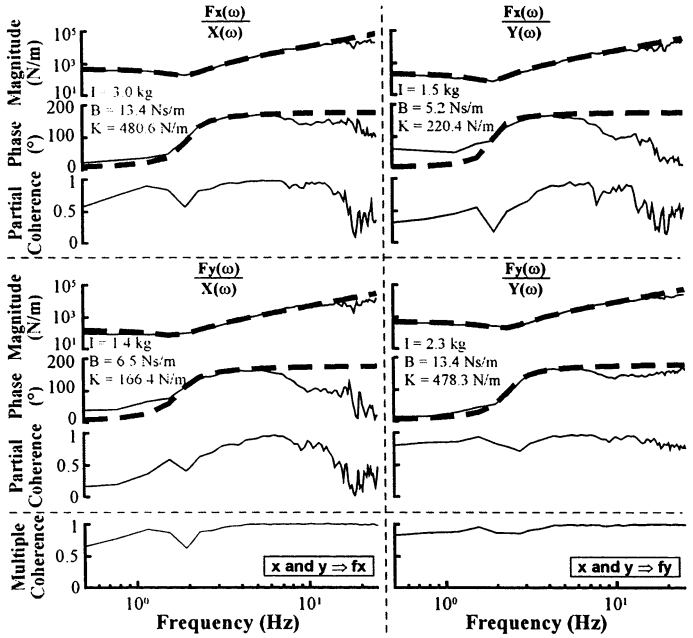

Fig. 7. Identification of a human arm. Elements of the elastic field are represented by their frequency responses (magnitude and phase) with the corresponding partial coherence and multiple coherence functions. The second order fits for the diagonal elements are illustrated by the dashed traces.

tion. The adjustable height and inclination features of the manipulator will allow characterization of the endpoint properties of the arm in planes containing more natural arm postures or movements (i.e. reaching overhead) than the horizontal plane conditions used in all previous studies. We have demonstrated that the manipulator can be used to accurately characterize several known linear systems having different elastic, viscous, and inertial properties. We therefore believe that this same experimental approach is capable of identifying unknown human upper extremity mechanical properties over a wide range of previously untested conditions. This information will contribute to the understanding of the neural control of movement, and aid in the development of rehabilitation interventions for disabled individuals.

The use of stochastic perturbations for the characterization of endpoint dynamic stiffness has several advantages over other types of perturbations (i.e. steps) used in previous studies. Stochastic perturbations are experimentally efficient, allowing many conditions to be examined in a single experimental session. This type of perturbation can be used to probe both static and dynamic properties, allowing simultaneous estimation of elastic, viscous, and inertial properties. Finally, stochastic perturbations are by nature unpredictable to human subjects, minimizing the significant problem of voluntary intervention.

As in all previous studies, the approach described here is limited to two dimensions. The system identification methods used here can be used for any number of inputs and any number of outputs, and thus do not limit the full characterization of limb stiffness. However, for a general description, a robotic arm capable of imposing three orthogonal forces and three orthogonal moments onto the endpoint in a controlled manner would be required. We have made a modest advance towards generating more global stiffness estimates by providing the capability to study the two-dimensional endpoint properties in different planes of movement.

Our current system uses endpoint position control, which is appropriate for studying posture but not movement. Other groups have studied the stiffness properties of the human arm during highly stereotyped movements using position control (Bennett et al., 1992), force control (Xu and Hollerbach, 1999), and impedance control (Gomi and Kawato, 1997). True measurement of stiffness during movement is limited by difficulties in providing true endpoint force control and in identification of time-varying systems with long memory dynamics as is the case for musculoskeletal systems.

The parameter estimates for all the characterized physical systems had errors ranging from 0.3 to 11%. Mass estimation errors (Fig. 6) were due in part to limitations in the resolution of the force measurements, especially for the smaller masses, and to out-of-plane vibrations of the manipulator arm. The air dashpot was actually nonlinear over its full velocity range, although it was linear over the more restricted range of velocities used here. The spring elasticity estimates were likely degraded by out-of-plane oscillations that occurred

during the applied perturbations due to the mass of the springs. Finally, we believe that the fitting procedure for obtaining elastic, viscous, and inertial parameters from the dynamic stiffness transfer functions accounts for a significant fraction of these observed errors. Although the least square error approach used to fit parameters to the transfer functions produced good overall fits, the estimated parameter values depended somewhat on the range of frequencies used in the fit. For example, more accurate estimates of elasticity could be obtained by limiting the fit to frequencies below resonance. However, such fits predicted higher frequency behavior poorly and produced inaccurate estimates of the other parameters (i.e. viscosity and inertia). We thus decided to fit all the parameters simultaneously over the full frequency range. Improved parameter fitting routines could be used in the future to address this problem. Despite these identified error sources, the parameter estimates obtained for the tested physical systems were actually quite accurate, demonstrating the validity of the methods developed here and their applicability in the characterization of human arm endpoint dynamic stiffness. Furthermore, the same methods used in characterizing the known physical systems were applied to obtain a single example of the endpoint dynamic stiffness properties of the human arm. The elastic, viscous and inertial parameter estimates obtained from second order model fits to the identified transfer functions agree with previous reports of the mechanical properties of the human arm.

In summary, we have validated the methods and demonstrated the ability to accurately characterize the dynamic stiffness properties of known systems and the ability to provide an example of the endpoint dynamic stiffness properties of the human arm. The methods developed here will be applied to the study of human arm posture and movement control over a wide range of functionally relevant conditions. The same methods will also be used in the development and improvement of rehabilitation techniques, such as functional electrical stimulation and muscle tendon transfer surgeries, that are used to restore movement in disabled individuals.

Acknowledgements

This work was supported by the Whitaker Foundation and by the Department of Veterans Affairs Rehabilitation Research and Development Service. We would like to thank Drs Patrick Crago, Randy Ellis, Ed Colgate and Roger Quinn for their helpful comments on robotic design and control. We would especially like to thank Michael Mahar of Mahar-Spar, Inc., who contributed significantly to the design of the manipulator and supervised its construction.

References

Acosta AM, Kirsch RF. Endpoint stiffness estimation for assessing arm stability. First Annual Conference of the International Functional Electrical Stimulation Society, Cleveland, OH, 1996a.

Acosta AM, Kirsch RF. A planar manipulator for the study of multi-joint human arm posture and movement control. IX Engineering Foundation Conference on the Biomechanics and Neural Control of Movement, Mt. Sterling, USA, 1996b.

Bennett DJ, Hollerbach JM, Xu Y, Hunter IW. Time-varying stiffness of human elbow joint during cyclic voluntary movement. Exp Brain Res 1992;88:433–42.

Chaffin DB, Andersson GBJ. Occupational Biomechanics, 2 edn. New York: Wiley, 1991, 518 pp.

Crago PE, Houk JC, Hasan Z. Regulatory actions of human stretch reflex. J Neurophysiol 1976;39:925–35.

Ford LE, Huxley AF, Simmons RM. The relation between stiffness and filament overlap in stimulated frog muscle fibres. J Physiol (Lond) 1981;311:219–49.

Gomi H, Kawato M. Equilibrium-point control hypothesis examined by measured arm stiffness during multijoint movement. Science 1996;272:117–20.

Gomi H, Kawato M. Human arm stiffness and equilibrium-point trajectory during multi-joint movement. Biol Cybern 1997;76:163–71.

Gomi H, Osu R. Task-dependent viscoelasticity of human multijoint arm and its spatial characteristics for interaction with environments. J Neurosci 1998;18:8965–78.

Gordon AM, Huxley AF, Julian FJ. The variation in isometric tension with sarcomere length in vertebrate muscle fibres. J Physiol (Lond) 1966;184:170–92.

Hoffer JA, Andreassen S. Regulation of soleus muscle stiffness in premammillary cats: intrinsic and reflex components. J Neurophysiol 1981;45:267–85.

Hogan N. The mechanics of multi-joint posture and movement control. Biol Cybern 1985;52:315–41.

Hollerbach JM, Flash T. Dynamic interactions between limb segments during planar arm movement. Biol Cybern 1982;44:67–77.

Houk JC. Regulation of stiffness by skeletomotor reflexes. Annu Rev Physiol 1979;41:99–114.

Huxley H. The working stroke of myosin crossbridges. Biophys J 1995;68:55S–56S; discussion 57S–58S.

Kearny RE, Hunter IW. System identification of human joint dynamics. Crit Rev Biomed Eng 1990;18:55–87.

Kirsch RF, Rymer WZ. Neural compensation for fatigue-induced changes in muscle stiffness during perturbations of elbow angle in human. J Neurophysiol 1992;68(2):449–70.

Kirsch RF, Boskov D, Rymer WZ. Muscle stiffness during transient and continuous movements of cat muscle: perturbation characteristics and physiological relevance. IEEE Trans Biomed Eng 1994;41:758–70.

Kojima H, Ishijima A, Yanagida T. Direct measurement of stiffness of single actin filaments with and without tropomyosin by in vitro nanomanipulation. Proc Natl Acad Sci USA 1994;91:12962–6.

Lacquaniti F, Soechting JF. Responses of mono- and bi-articular muscles to load perturbation of the human arm. Exp Brain Res 1986a;65:135–44.

Lacquaniti F, Soechting JF. Simulation studies on the control of posture and movement in a multi-jointed limb. Biol Cybern 1986b;54:367–78.

Lagarias J, Reeds J, Wright M, Wright P. Convergence properties of the Nelder–Mead simplex method in low dimensions. SIAM J Optim 1998;9:112–47.

Matthews PBC. The dependence of tension upon extension in the stretch reflex of the soleus muscle of the decerebrate cat. J Physiol 1959;147:521–46.

McIntyre J, Mussa-Ivaldi FA, Bizzi E. The control of stable postures in the multijoint arm. Exp Brain Res 1996;110:248–64.

Milner TE, Cloutier C. Compensation for mechanically unstable loading in voluntary wrist movement. Exp Brain Res 1993;94(3):522–32.

Mussa-Ivaldi FA, Hogan N, Bizzi E. Neural, mechanical, and geometric factors subserving arm posture in humans. J Neurosci 1985;5:2732–43.

Nichols TR, Houk JC. Reflex compensation for variations in the mechanical properties of a muscle. Science 1973;181:182–4.

Nichols TR, Houk JC. Improvement in linearity and regulation of stiffness that results from actions of stretch reflex. J Neurophysiol 1976;39:119–42.

Osu R, Gomi H. Multijoint muscle regulation mechanisms examined by measured human arm stiffness and EMG signals. J Neurophysiol 1999;81:1458–68.

Perreault EJ, Kirsch RF, Acosta AM. Multiple-input, multiple-output system identification for characterization of limb stiffness dynamics. Biol Cybern 1999;80:327–37.

Rack PM, Westbury DR. The effects of length and stimulus rate on tension in the isometric cat soleus muscle. J Physiol (Lond) 1969;204:443–60.

Shadmehr R, Mussa-Ivaldi FA, Bizzi E. Postural force fields of the human arm and their role in generating multijoint movements. J Neurosci 1993;13:45–62.

Soechting JF, Lacquaniti F. Quantitative evaluation of the electromyographic responses to multidirectional load perturbations of the human arm. J Neurophysiol 1988;59:1296–313.

Tsuji T, Morasso PG, Goto K, Ito K. Human hand impedance characteristics during maintained posture. Biol Cybern 1995;72:475–85.

Xu Y, Hollerbach JM. Identification of human joint mechanical properties from single trial data. IEEE Trans Biomed Eng 1998;45:1051–60.

Xu Y, Hollerbach JM. A robust ensemble data method for identification of human joint mechanical properties during movement. IEEE Trans Biomed Eng 1999;46:409–19.

Xu Y, Hunter IW, Hollerbach JM, Bennett DJ. An airjet actuator system for identification of the human arm joint mechanical properties. IEEE Trans Biomed Eng 1991;38:1111–22.